Human Molecular Genetics, 2010, Vol. 19, No. 6 **1088–1097**
doi:10.1093/hmg/ddp580
Advance Access published on January 4, 2010

Neuronopathic Gaucher disease in the mouse: viable combined selective saposin C deficiency and mutant glucocerebrosidase (V394L) mice with glucosylsphingosine and glucosylceramide accumulation and progressive neurological deficits

Ying Sun[1,4], Benjamin Liou[1,4], Huimin Ran[1,4], Matthew R. Skelton[2,4], Michael T. Williams[2,4], Charles V. Vorhees[2,4], Kazuyuki Kitatani[6], Yusuf A. Hannun[6], David P. Witte[3,5], You-Hai Xu[1,4] and Gregory A. Grabowski[1,4,*]

[1]The Division of Human Genetics, [2]Division of Neurology, [3]Division of Pediatric Pathology, Cincinnati Children's Hospital Medical Center, [4]Department of Pediatrics, [5]Department of Pathology, University of Cincinnati College of Medicine, Cincinnati, OH 45229-3039, USA and [6]Department of Biochemistry and Molecular Biology, Medical University of South Carolina, Charleston, SC 29425, USA

Received July 15, 2009; Revised and Accepted December 23, 2009

Gaucher disease is caused by defective acid β-glucosidase (GCase) function. Saposin C is a lysosomal protein needed for optimal GCase activity. To test the *in vivo* effects of saposin C on GCase, saposin C deficient mice (C−/−) were backcrossed to point mutated GCase (V394L/V394L) mice. The resultant mice (4L;C*) began to exhibit CNS abnormalities ∼30 days: first as hindlimb paresis, then progressive tremor and ataxia. Death occurred ∼48 days due to neurological deficits. Axonal degeneration was evident in brain stem, spinal cord and white matter of cerebellum accompanied by increasing infiltration of the brain stem, cortex and thalamus by CD68 positive microglial cells and activation of astrocytes. Electron microscopy showed inclusion bodies in neuronal processes and degenerating cells. Accumulation of p62 and Lamp2 were prominent in the brain suggesting the impairment of autophagosome/lysosome function. This phenotype was different from either V394L/V394L or C−/− alone. Relative to V394L/V394L mice, 4L;C* mice had diminished GCase protein and activity. Marked increases (20- to 30-fold) of glucosylsphingosine (GS) and moderate elevation (1.5- to 3-fold) of glucosylceramide (GC) were in 4L;C* brains. Visceral tissues had increases of GS and GC, but no storage cells were found. Neuronal cells in thick hippocampal slices from 4L;C* mice had significantly attenuated long-term potentiation, presumably resulting from substrate accumulation. The 4L;C* mouse mimics the CNS phenotype and biochemistry of some type 3 (neuronopathic) variants of Gaucher disease and is a unique model suitable for testing pharmacological chaperone and substrate reduction therapies, and investigating the mechanisms of neuronopathic Gaucher disease.

INTRODUCTION

Gaucher disease is caused by inherited deficiency of acid β-glucosidase (GCase). The mutations in the GCase gene [human (GBA), mouse (*gba*)] lead to defective hydrolysis of glucosylceramide (GC) that results in the storage of GC in the liver, spleen, bone marrow and central nervous system (1,2). Clinically, two major categories of Gaucher disease

*To whom correspondence should be addressed at: Division of Human Genetics, Cincinnati Children's Hospital Medical Center, 3333 Burnet Avenue, MLC 4006, Cincinnati, OH 45229-3039, USA. Tel: +1 5136367290; Fax: +1 5136362261; Email: greg.grabowski@cchmc.org

© *The Author 2010. Published by Oxford University Press.*
This is an Open Access article distributed under the terms of the Creative Commons Attribution Non-Commercial License (http://creativecommons.org/licenses/by-nc/2.5), which permits unrestricted non-commercial use, distribution, and reproduction in any medium, provided the original work is properly cited.

have been delineated, non-neuronopathic and neuronopathic. Type 1 includes the non-neuropathic variants, whereas types 2 and 3 encompass the acute and subacute neuronopathic variants (2). Type 2 is rare (<1/500 000 live births) and manifests progressive neuronopathic disease within the first 2–3 months with median survival of <1 year (3–5). Death results from severe progressive CNS and lung involvement. Type 3 is more slowly progressive, rare (1/100 000 live births) and has a wide spectrum of phenotypes extending from early severe visceral and mild neuropathic variants to mild visceral disease with uncontrollable seizures later in adolescence (2). In the neuronopathic variants, GC and glucosylsphingosine (GS) accumulations have been documented in the brain (6–8). Unlike the visceral disease, pathogenesis in the CNS is not related to large storage cell (macrophages) accumulations but, rather, to neuronal death/drop-out that is propagated by toxic effects of GS and/or GC (3,9,10).

Saposins (A, B, C and D) are small (80 amino acids) protein enhancers of specific glycosphingolipid (GSL) hydrolase activities (11). They derive from a single precursor protein, prosaposin, by proteolysis in the late endosome and lysosome (12). Among the four saposins, only saposin C has activation and anti-proteolytic protective effects toward GCase (13). Deficiency of saposin C leads to a variant form of Gaucher disease with GC accumulation in macrophages and in the CNS (14). Saposin C's mode of GCase activation is related to induced alterations of the membrane bilayer that facilitate enzyme and substrate interaction (15). Although the involvement of saposin C in the degradation of GC is well-established *in vitro* (11,16), the *in vivo* mechanisms of its action are not fully understood.

Knockout of the *gba* locus in mice abolishes GCase activity and leads to neonatal death (17). In brains of these GCase knockout mice, GS levels are increased by ~100-fold (8) along with the increases of GC (18). Although neuronal loss is not observed, some GC storage in neurons is observed in spinal cord and brain stem (18). Recently, more viable GCase mouse models with acute neuronopathic Gaucher disease have been generated (19,20). By either rescue of the skin of mice that are null in all other cells or specifically knocking out *gba* only in neurons, longer lived (2–3 weeks) acute neuronopathic variants were created as mimics of human type 2 Gaucher disease (19,20). However, the foreshortened lifespan limits biochemical and neuronopathological studies of the disease progression. Additional efforts were taken to create Gaucher disease models include knock-ins of point mutations (e.g. V394L, D409H or D409V) with or without combinations with hypomorphic prosaposins (14). The latter models develop storage cells in visceral and GC accumulation in visceral, but have complex GSL accumulations in the CNS due to prosaposin deficiency (21). A principle impediment to understanding the pathophysiology and therapeutic developments for the CNS variants has been the lack of viable neuronopathic mouse models with sufficient lifespans.

In this study, a new mouse model was generated by cross-breeding of the V394L GCase homozygote into the saposin C null (C−/−) mouse. Deficiency of saposin C led to additional reductions of the V394L GCase and increases of GC and GS levels. This viable model developed neurological deficits analogous to subacute neuronopathic Gaucher disease.

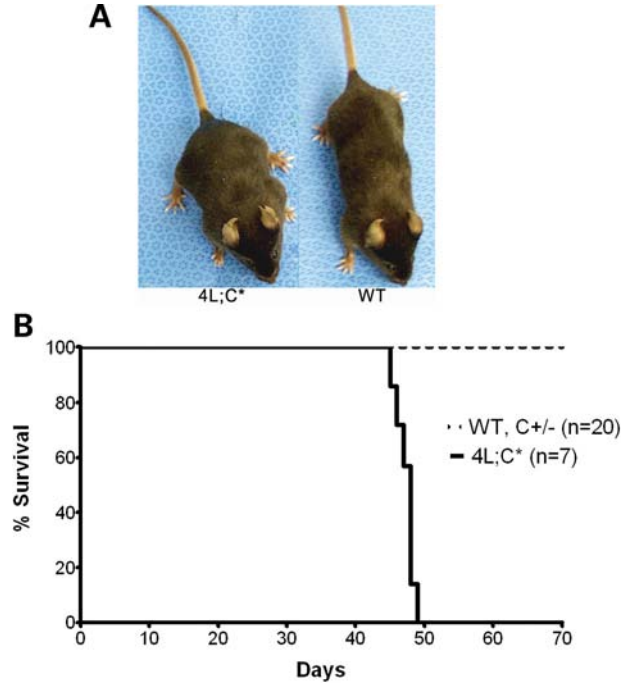

Figure 1. Phenotypes and lifespan of 4L;C* mice. (**A**) 4L;C* mouse showed hindlimb paresis and duck waddling by 47 days. They weighed 25% less than control mice. (**B**) Kaplan–Meier survival curves for 4L;C* and control (WT and C+/−) mice. Average lifespan of 4L;C* mice was 48 days.

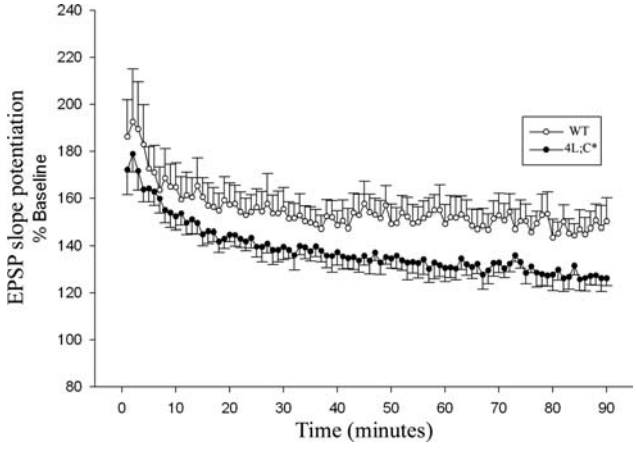

Figure 2. Electrophysiology analyses of long-term potentiation (LTP). The slope of resulting EPSPs from the parasagittal sections (350 μm) of hippocampal CA1 region was recorded. The slopes of the EPSP (LTP) in 35 days 4L;C* (black circle) was significantly ($P < 0.05$) decreased compared with WT (open circle) mice after recording for 90 min following stimulation. WT, $n = 6$ mice; 4L;C*, $n = 8$ mice.

RESULTS

Generation of 4L;C* mice

The 4L/4L mice have ~10% WT GCase activity and no apparent CNS abnormalities (22). Saposin C−/− mice showed ~60% of WT GCase activity and protein in several tissues and developed a CNS phenotype around 1 year of age (23).

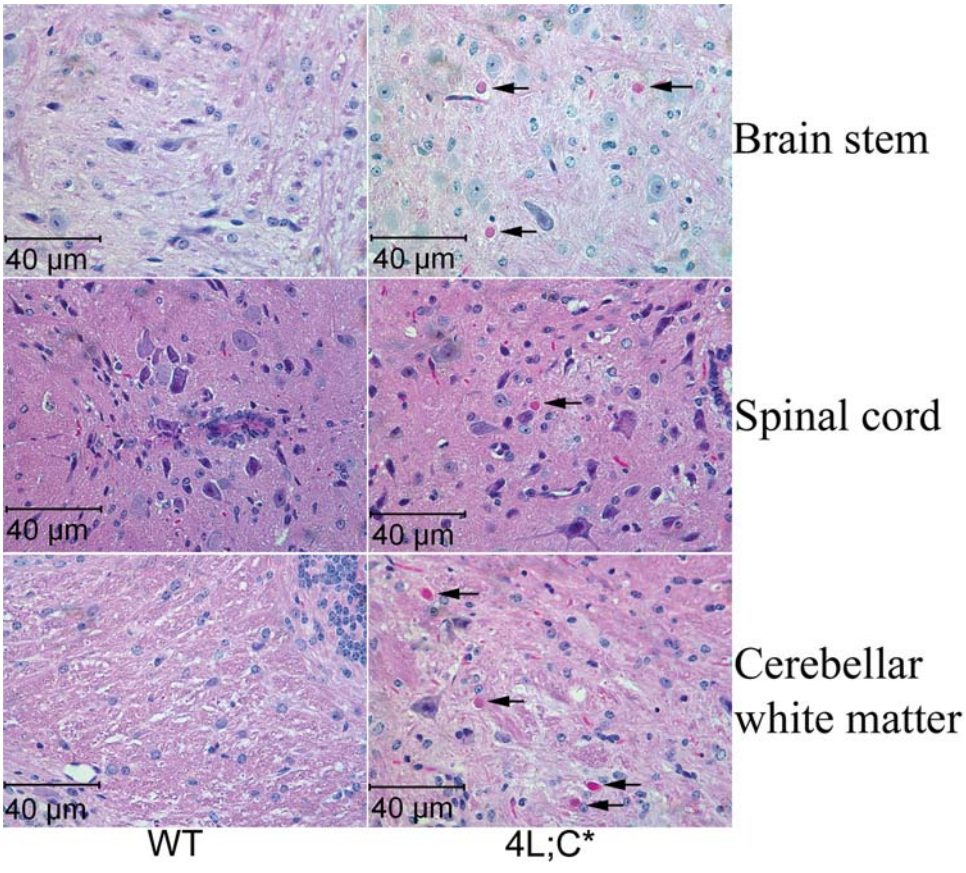

Figure 3. Neuropathology in 4L;C* mice. The sections from 46-day 4L;C* mice were stained with H&E. Axonal degeneration (arrows) was present in brain stem, spinal cord and white matter of cerebellum in 4L;C* mice. WT brain stem, spinal cord and cerebellum had normal morphology.

The 4L;C* mice were born in normal sized litters with expected Mendelian ratios for the offspring. They began showing phenotypic abnormalities and neurological deficits ~30 days and died by ~48 days (Fig. 1) due to inability to eat and drink. At ~35 days, the 4L;C* mice had outwardly splayed hind limbs and their stomachs dragged when walking. The gait of 4L;C* mice was a duck-like waddling due to the splaying of their hindlimbs and apparent stiffness and progressive bradykinesia, relative to WT, that progressed until death when the 4L;C* mice were nearly immobile (Fig. 1). Also, grip weakness of the 4L;C* mice was progressive. By age 43–48 days, they weighed 25% less than the control groups (C+/−, 4L/4L, 4L/4L;C+/− and wt/wt; wt/wt) with an average of 17.2 g compared with 23.0 g in controls. All control mice had weights and lifespans similar to WT.

Electrophysiology analyses

The neuronal cells of hippocampal sections in the brain were recorded as excitatory postsynaptic potential (EPSP) slope potentiation (LTP, long-term potentiations) on a MED64 array chamber in the warm artificial cerebral spinal fluid. After accounting for a baseline of activity, the hippocampi from 4L;C* mice at 35 days showed significant ($P < 0.05$) decreases of LTP, compared with the WT mice (Fig. 2), suggesting an overall reduction of hippocampal plasticity in 4L;C* mice.

Histological analyses

In the hematoxylin and eosin (H&E) stained sections, axonal degeneration (Fig. 3 arrow) was evident in the brain stem, spinal cord and white matter of cerebellum of 4L;C* mice at 46 days. The anti-CD68 positive microglial cells were numerous in the brainstem, basal ganglion, thalamus, hypothalamus, cerebral cortex and spinal cord (Fig. 4A). Moderate astrogliosis as evidenced by anti-GFAP positivity was observed in the midbrain, brainstem, multiform layer of cerebral cortex, thalamus, corpus collosum, cerebellum and spinal cord (Fig. 4B). The enhanced microglial cell activation and astrogliosis indicates proinflammation in 4L;C* CNS. Lamp2 is a membrane protein located in the late endosome and lysosome (24). Lamp2 immunoreactivity was increased in thalamus (Fig. 5), brain stem, basal ganglion and white matter of cerebellum. P62/sequestosome 1 is involved in autophagic clearance of ubiquitinated proteins (25). Enhanced p62 signals were intense in the thalamus (Fig. 5) and scattered p62 positive cells were in brain stem, basal ganglion and cortex. Accumulation of p62 was found in the neurons and astrocytes, but not in the microglial cells (Fig. 5B). These results suggest impairment of autophagosome and lysosome apparatus in 4L;C* brain. Tunnel assays in 4L;C* CNS tissues were negative. No histological abnormalities were found in the visceral tissues of 4L;C* mice. The brain and spinal cord morphology in saposin C−/− and 4L/4L mice were normal at 46 days.

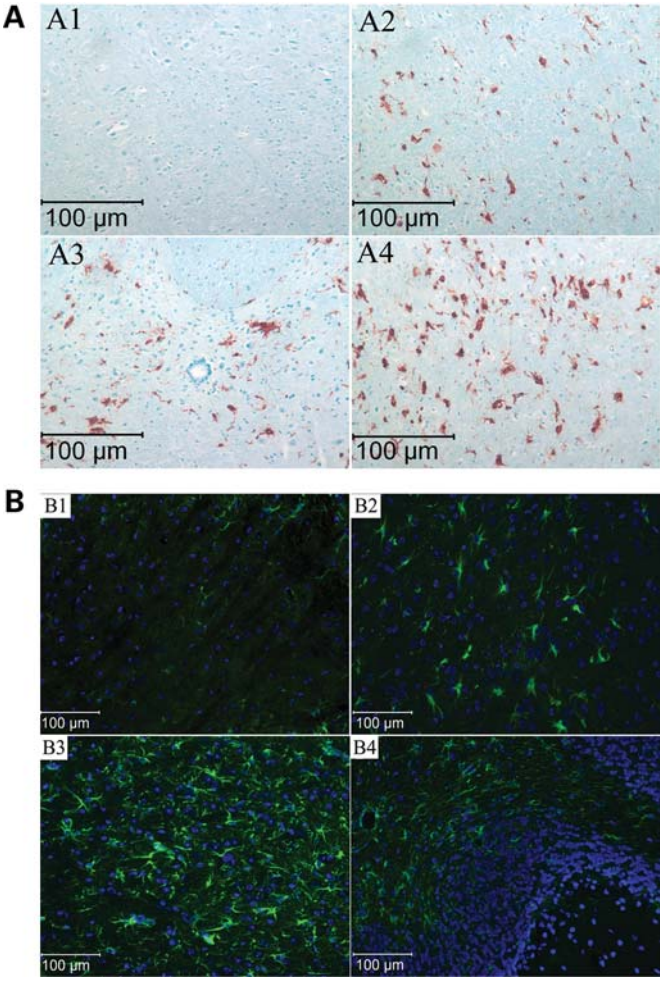

Figure 4. Neuroinflammation in 4L;C* mice. (**A**) CD 68 staining (brown) in 46-day 4L;C* and WT mice. [A1]WT brain stem had background levels of CD68 staining. CD68 positive staining demonstrated activation of macrophage/microglial cells in 4L;C* brain stem [A2], spinal cord [A3] and thalamus [A4]. Methyl green (green) was used to stain cell nuclei. (**B**) GFAP staining (green) in 46 days 4L;C* and WT mice. [B1] WT brain stem had background level GFAP staining. Enhanced GFAP staining presented in 4L;C* brain stem [B2], thalamus [B3] and cerebellum [B4]. Cell nuclei were stained with DAPI (blue).

Ultrastructural studies of CNS regions revealed the inclusion materials in the neuronal cell processes from brain stem, spinal cord, white matter of cerebellum and midbrain regions of 43-day-old mice (Fig. 6). The inclusions were visualized as electron dense and lucent materials in axonal processes. The storage materials were heterogeneous and coarsely granular. The ultrastructure shows axonal cell processes expanded by numerous tightly packed single-membrane bound bodies consistent with phagolysosomes (Fig. 6C, E and F). The sequestered materials range from dense osmiophilic undigested material to partially digested electron-lucent material. In the hippocampus, dendritic processes contained membrane-like material. Separation of myelin sheath was evident in spinal cord (Fig. 6C), brainstem and midbrain regions of 43-day 4L;C* mice. Degenerating cells and swollen cell processes were identified in cortex and hippocampal regions. In many processes, the subcellular organelles were compressed to the periphery by the accumulating storage materials. The general appearance of the soma of neurons was normal in 4L;C* mice (Fig. 6D).

GCase levels in 4L;C* mice

The GCase activity in 4L;C* was reduced to $<10\%$ of WT in liver, lung, spleen, brain and cultured skin fibroblasts. These levels were 40–60% of those in the respective tissues of 4L/4L mice (Fig. 7A). The GCase activity (WT enzyme) in saposin C−/− mice was ∼60% of those in saposin C+/+ mice (Fig. 7A). Liver GCase protein was determined by immunoblot using anti-mouse GCase antibody. Consistent with the activity data, 4L;C* mice had ∼40% of 4L/4L levels GCase protein levels (Fig. 7B). These results indicate that the deficiency of saposin C led to a concordant reduction in mutant V394L GCase protein and activity.

GSL analyses

Relative to WT mice, marked increases of GS were present in cerebral cortex (∼20-fold) and midbrain (∼30-fold) from 43-day-old 4L;C* mice. Levels of GS also were massively increased in 43-day-old 4L;C* mouse lung and liver (Fig. 8A). GC levels were increased ∼3-fold in the liver and lung, and by ∼1.5-fold in the cortex and midbrain relative to WT. Increases of ceramide (1.6-fold) and sphingosine (3.4-fold) were found only in the liver of 4L;C*. Lactosylceramide levels was not significantly altered in 4L;C* mice. No excess accumulations of GC and GS were detected in 10 weeks 4L/4L and 13 months C−/− mouse brains (data not shown). Elevated GC (1.3-fold) and GS (6.5-fold) were detected in 4L;C* skin at 14 days.

GSL was analyzed in hippocampal tissue from 44-day-old mice. Both GC (3.4-fold) and GS (132-fold) were elevated in 4L;C* mice (Fig. 8C). Galactosylceramide (GalCer) levels in 4L;C* were at WT levels, indicating normal GalCer metabolism in 4L;C* mice. This result suggests a correlation of substrate accumulation with abnormal LTP in 4L;C* mice.

DISCUSSION

Neuronopathic Gaucher disease variants present with brainstem, cerebellar, thalamic, cerebral cortical and substantia nigra involvement, but the degrees of involvement and affected regions vary among the patients (26–28). The neuropathological involvement has been correlated with the accumulation of GS and GC (6,26) with increased GS mostly associated with the widespread neuron loss in Gaucher disease type 2 (7,29,30). This neuronal loss is also associated with astrogliosis and microglial nodules (6,27). Additionally, GS suppresses neuritogenesis (31). *In vitro* GC addition to microsomes from type 1, 2 or 3 Gaucher patients stimulated agonist-induced Ca^{2+} release and this alteration correlated with the level of GC accumulation (32). GS also directly augments the Ca^{2+} release in an agonist-independent manner in such microsomes (32,33). This Ca^{2+} release, presumably from endoplasmic reticulum, has been speculated to be responsible for neuron cell death due to GC or GS increases (34). Furthermore,

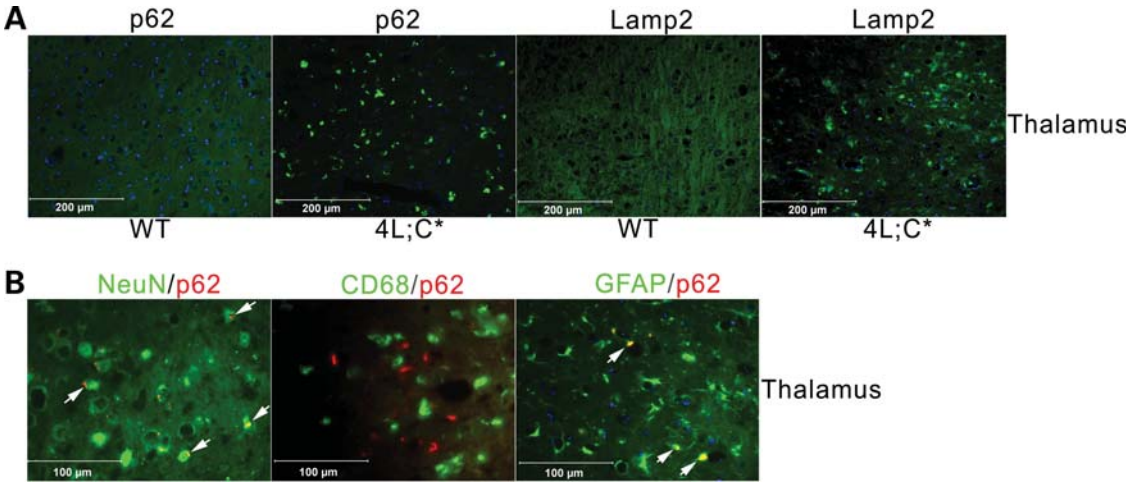

Figure 5. Accumulation of p62 and Lamp2 in 4L;C* thalamus. (**A**) Frozen sections from 46-day 4L;C* and WT mice were stained with anti-p62 and anti-Lamp2 antibodies, respectively. Both p62 (green) and Lamp2 signals (green) were increased in thalamus of 4L;C* brain relative to the WT control. (**B**) Colocalization of p62 in neuron, astrocyte or microglial cells in the thalamus of 4L;C* brain. Accumulation of p62 (red) was in neuron (green) stained by anti-NeuN antibody and astrocyte (green) stained with anti-GFAP antibody. Arrows point the p62 containing cells. Yellow color cell shows the overlapping of p62 and GFAP or NeuN. p62 (red) was not localized in CD 68 positive microglial cells (green). DAPI (blue) in anti-fade was used for cell nuclei staining.

hippocampal CA2-4 regions are significantly involved by neuronal injury in neuronopathic Gaucher disease variants (30). Here, the neuronal deficit in 4L;C* mice was likely caused by excess levels of GS and GC as well as the striking inclusions in axonal and neuronal processes. Furthermore, 4L;C* mice showed impaired hippocampal LTP that correlated with substrate accumulation and abnormal neuronal processes. Negative Tunnel assays in 4L;C* CNS tissues indicate that apoptosis was not the cause of neurodegeneration. The accumulation of p62, an autophagic receptor that mediates autophagic degradation of ubiquitinated proteins (25) and enhanced Lamp2 expression suggest an impairment of protein degradation in the autophagosome and lysosome system that could be the cause of neurodegeneration in this model.

Comparisons of the saposin C−/− mice and the 4L;C* mice provide insights into the function of saposin C and GCase. Importantly, saposin C provides a proteolytic protective effect for GCase within the lysosome and that its presence is required for the full activity of the enzyme. Here, the singular absence of saposin C led to further decreases in V394L mutant GCase activity as measured *in vitro*. This GCase protein level was also decreased indicating an increased instability or susceptibility of the mutant protein to proteolysis. Because of this decrease in GCase activity from ∼15 to ∼6% of WT levels, a new phenotype emerged with primarily central nervous system disease and with biochemical evidence of GC and GS storage in the viscera. Furthermore, the reduced V394L GCase activity in the brain was below a threshold to prevent the development of central nervous system disease, since neither the V394L homozygote nor the saposin C−/− mice themselves develop progressive central nervous system disease in the time frame of these studies.

A curious finding was that the level of GC in the brain had only minor changes, unlike the level of GS that showed major increases. GS is known to be highly toxic to cells, particularly neurons (31), and the elevated GS levels led to selective deterioration of the central nervous system in the 4L;C* mice. Although, the levels of GS in visceral tissues, on a fold basis, were similar to or greater than those in the CNS, the visceral organs do not show any major histological abnormalities. The lipid abnormalities were detectable only using MS. Thus, it appears that the visceral tissues are relatively resistant or insensitive to the toxic effects of GS. There is a much greater toxicity to similarly raised levels of GS for CNS cells. This difference in sensitivity may relate to the fact that neurons and glial cells in central nervous system are more vulnerable to GSLs accumulation than the cells in the liver and some other visceral tissues. Within the central nervous system, this disease process is also selective with specific involvement of neurons and some cells within the spinal cord while leaving much of the white matter uninvolved.

It is also clear that saposin C interacts functionally with both WT and mutant GCases. In both the saposin C−/− mouse with WT or with V394L GCases, the amount of enzyme protein present in the central nervous system is diminished compared with saposin C+/+ animals. The amount of WT GCase in saposin C−/− mice appears to be sufficient for the maintenance of central nervous system function in a normal state for periods >12 months and that the eventual phenotype is not clearly related to the accumulation of GC or GS within the CNS. Thus, the axonal degeneration and other histological abnormalities seen in the saposin C−/− mouse must relate to other intrinsic functions of saposin C, unrelated to its activity in promoting optimal GCase function (23). In contrast, the additional decrease in V394L activity caused by the absence of saposin C is below a threshold necessary for the protection of the central nervous system from GS toxicity. The early demise of the 4L;C* mice (48 days) compared with the longer lifespan of the saposin C−/− mice (>20 months), suggests that the toxic effects may be attributed to GS.

An interesting question is the differential accumulation of GS compared with GC in the brains of 4L;C* mice. Possible explanations include either functions related to saposin C or to

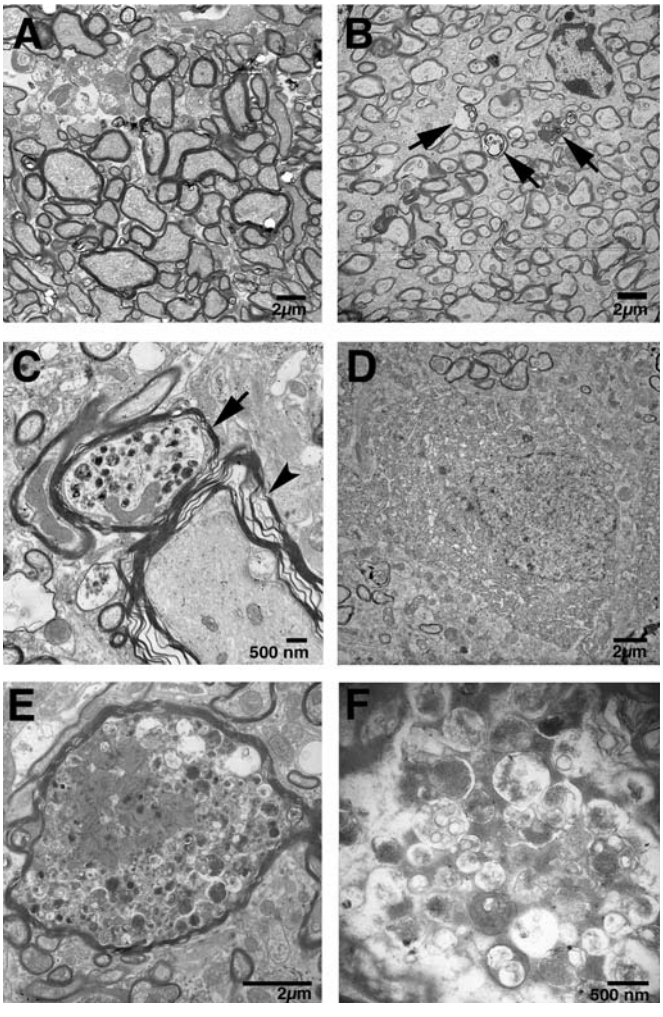

Figure 6. Ultrastructural features of 4L;C* CNS. (**A**) Normal midbrain morphology in 43 day WT. (**B**) Axonal inclusions (arrows) were in 43-day 4L;C*. (**C**) 4L;C* spinal cord showed storage materials in axonal process (arrow) and separation of myelin layers (arrowhead). (**D**) Brain stem of 4L;C* had normal neuron. (**E**) The white matter of cerebellum in 4L;C* mice contained a complex accumulation materials in axonal process. (**F**) Higher magnification of the complex accumulation in cerebellar axons showed amorphous granular inclusions of variable density. The storage materials are heterogeneous and coarsely granular.

the mutant enzyme V394L or both. Saposin C could affect substrate specificity and enhance the activity of GCase to a greater degree toward the deacylated analog, GS, compared with GC. This will be investigated in future studies. An alternative explanation is that the V394L has a preference for GS or GC substrates. GS has an affinity (as measured by K_i) for V394L that is ~4- to 5-fold decreased compared with WT, and that GC has a normal binding constant for this enzyme (Liou and Grabowski, unpublished data). This suggests a potentially pure kinetic effect of a diminished enzymatic activity in which, once below a threshold, GS, because of its poor binding, cannot engage V394L GCase and cannot be hydrolyzed, whereas GC can. Vaccaro *et al*. (35) showed that the k_{cat} for GS was ~100-fold less than that for GC using purified WT GCase. If this also applies to the V394L enzyme and the binding constant is diminished, the accumulation of GS could be explained on the basis of a kinetic phenomenon, based on the decreased ability of V394L to cleave the less preferred substrate.

Finally, the studies here address the question of whether the toxic agent in neuronopathic Gaucher disease is GC or GS. The 4L;C* mouse accumulates GS to greater relative levels than GC; 4L;C* is nearly a pure GS storage disease that leads to central nervous dysfunction and eventual death. As a pure GC storage disease of CNS is not available, the question of this lipid's toxicity alone cannot be directly addressed. However, the *in vitro* studies showing toxicity of galactosylsphingosine and GS translate reasonably well to their CNS animal models, i.e. the twitcher mouse and the 4L;C* mouse, respectively. The *in vivo* toxicity of GS to neurons remains to be clarified. It will be important to address whether a diminution in GS can occur by the use of GC synthase inhibitors, and thereby diminish toxicity of GS. If it is true that GC synthase is responsible for all or most of the synthesis of GC and GS, compounds that inhibit this synthase could be therapeutic to the neuropathic forms of Gaucher disease.

MATERIALS AND METHODS

Materials

The following were from commercial sources: NuPAGE 4–12% Bis-Tris gel, NuPAGE MES SDS running buffer, Anti-GFAP mouse monoclonal antibody conjugated Alexa Fluor 488 (Invitrogen, Carlsband, CA, USA). 4-Methyl-umbelliferyl-β-D-glucopyranoside (4MU-Glc; Biosynth AG, Switzerland). Sodium taurocholate (Calbiochem, La Jolla, CA, USA). Rat anti-mouse CD68 monoclonal antibodies (Serotec, Oxford, UK). M-PER Mammalian Protein Extraction Reagent, ImmunoPure immobilized Protein G and BCA Protein Assay reagent (Pierce, Rockford, IL, USA). Hybond^{TM}-ECL^{TM} nitrocellulose membrane and ECL detection reagent (Amersham Biosciences, Piscataway, NJ, USA). Anti-fade/DAPI, Methyl green, ABC Vectastain and Alkaline Phosphatase Kit II (Black) (Vector Laboratory, Burlingame, CA, USA). Anti-pig GFAP mouse monoclonal antibody (Sigma, St Louis, MO, USA). Anti-recombinant p62/SQSTM1 mouse monoclonal antibody (Abnova, Taipei, Taiwan). Anti-mouse NeuN mouse monoclonal antibody conjugated Alex Fluor 488 (Millipore, Temecula, CA, USA). Anti-mouse Lamp2 rat monoclonal antibody (Abcam, Cambridge, MA, USA).

Animal care

Saposin C deficient (C−/−) mice (23) were generated by introducing a Cys → Pro substitution in the saposin C region of prosaposin. Substitution of this conserved cysteine (Cys) breaks one of the three disulfide bridges of saposin C and resulted in the specific deficiency of saposin C. This strategy has been used to produce several single and double saposin deficient mice (36,37). Saposin C−/− were cross-bred with point mutated GCase V394L homozygotes (4L/4L) (22) to generate C−/−;4L/wt and C+/−;4L/4L. 4L;C* mice (C−/−;4L/4L) were produced by intercrossing C−/−; 4L/wt and C+/−;4L/4L. The strain background of 4L;C* was C57BL/6J/129SvEV. The mice were maintained in microisolators in accordance with institutional guidelines

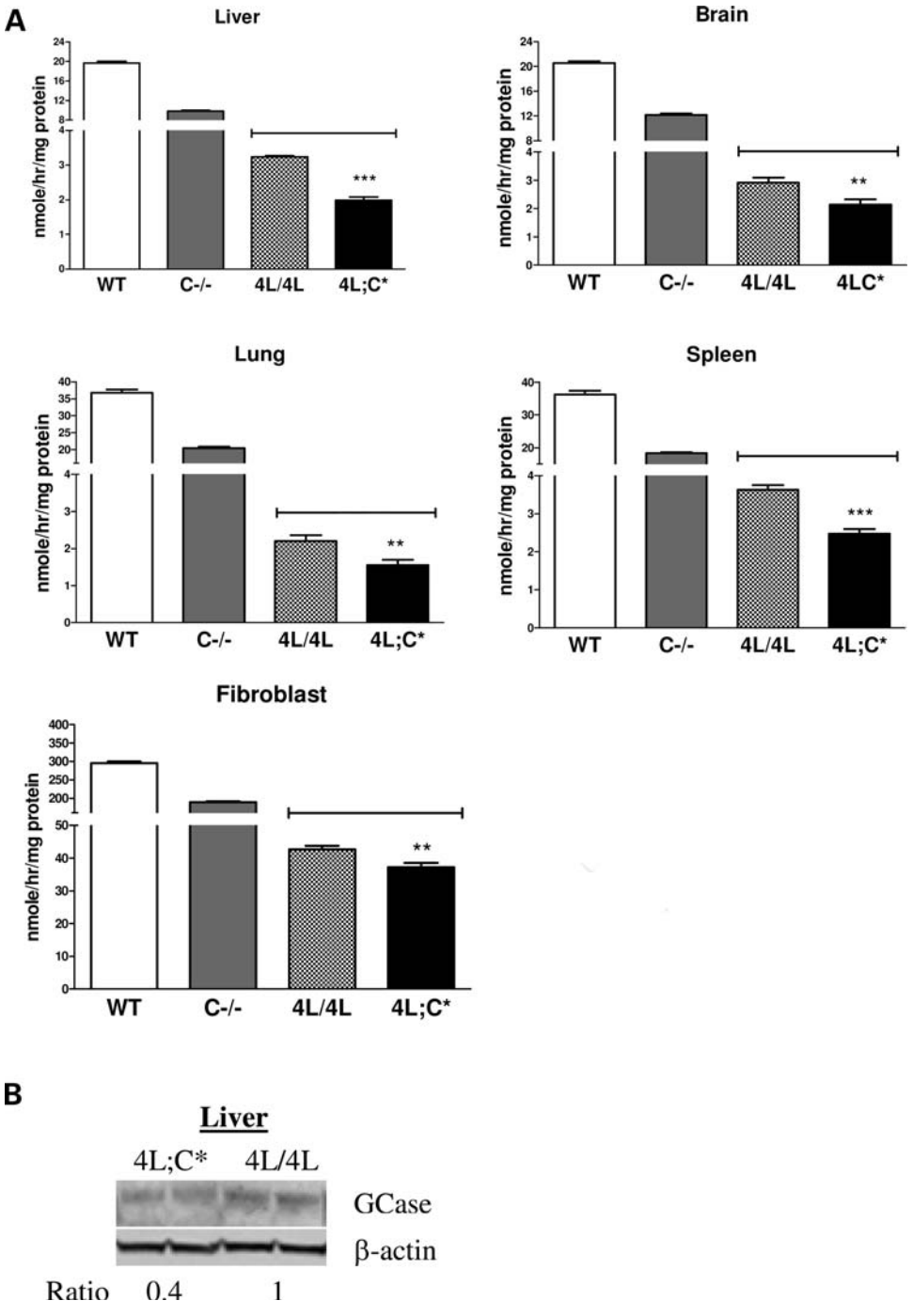

Figure 7. GCase activity and protein in 4L;C* mice. (**A**) The activities of GCase decreased significantly in 4L;C* liver, brain, lung, spleen and fibroblasts compared with 4L/4L, C−/− and WT tissues ($n = 3$). (**B**) GCase protein was decreased in 4L;C* livers by immunoblot analyses using anti-mouse GCase antibody. GCase protein level was normalized to β-actin signals in the same sample and presented as ratio relative to 4L/4L. A representative immunoblot is shown. The data represented the means ± SE for three mice assayed in duplicates. $^{**}P < 0.01$; $^{***}P < 0.001$.

under IACUC approval at Cincinnati Children's Hospital Research Foundation.

Tissue collection and immunohistochemistry

The 4L;C* and strain-matched WT mice were subjected to CO_2 narcosis and then, perfused with saline followed by 4% paraformaldehyde before tissue dissection. The tissues were fixed in 10% formalin or 4% paraformaldehyde and processed for paraffin or frozen blocks, respectively. Paraffin sections of brain were stained with H&E. Karnovsky's fixative was used for ultrastructural studies. CD68 monoclonal antibody staining was as described (14). Frozen sections were stained with mouse anti-pig glial fibrillary acidic protein (GFAP) that

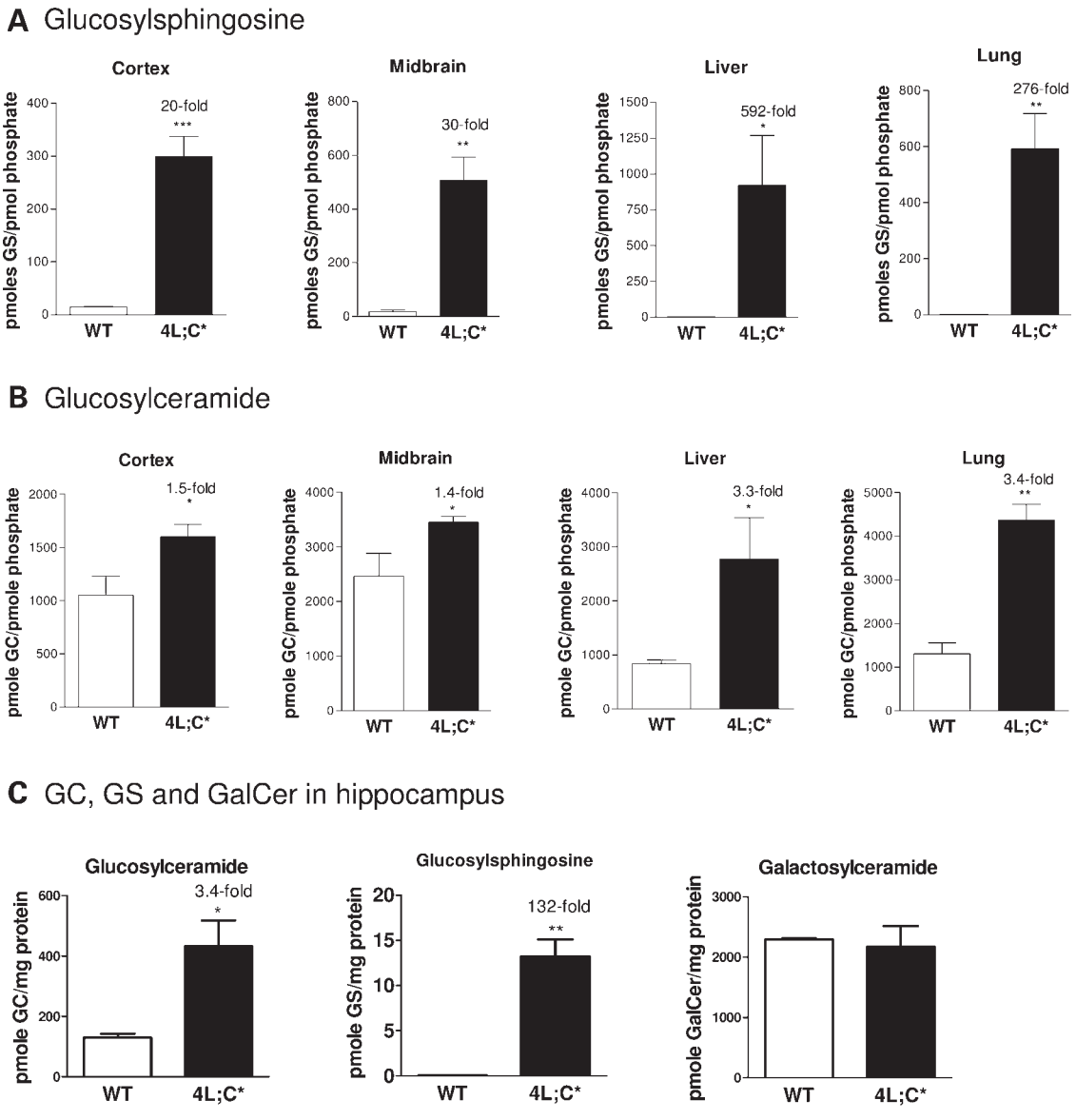

Figure 8. LC/MS analyses of GC and GS. (**A**) GS levels showed marked increases (20- to 600-fold) by 43 days in 4L;C* cortex, midbrain, liver and lung. (**B**) Increases of GC (1.5- to 3-fold) were detected in 4L;C cortex, midbrain, liver and lung. These GC and GS levels were normalized to phosphate content in the same sample and presented as fold change relative to WT controls. (**C**) Both GC (3.4-fold) and GS (132-fold) levels were significantly increased in 4L;C* hippocampus relative to WT. GalCer in 4L;C* hippocampus was at WT level. The hippocampal GC, GS and GalCer levels were normalized to mg protein in the same sample. The data were analyzed by Student's *t*-test. $^{*}P < 0.05$; $^{**}P < 0.01$, $^{***}P < 0.001$ ($n = 3$ mice).

detects astrocytes, mouse anti-recombinant p62 that is an autophagic receptor and rat anti-mouse Lamp2 that is a late endosome and lysosomal membrane protein. Biotinylated goat anti-mouse followed by streptavidin-conjugated fluorescent 488 (green) and goat anti-rat conjugated to FITC were applied to the sections. Both mouse anti-pig GFAP and mouse anti-recombinant p62 antibodies have reactivities in the mouse tissues (38,39). Colocalization of p62 in neuron, astrocyte or microglial cells was carried out on frozen sections using mouse anti-recombinant p62 (1:100) followed by biotinylated goat anti-mouse and streptavidin-conjugated fluorescent 610 (red). Mouse anti-NeuN conjugated to Alexa Fluor 488 (1:100), mouse anti-GFAP conjugated to Alexa Fluor 488 (1:100) or rat anti-CD68 (1:100) were applied as marker for neuron, astrocyte or microglial cells, respectively. Rat anti-CD68 was detected by biotinylated goat anti-rat and streptavidin-conjugated fluorescent 488 (green). DAPI (blue) in anti-fade were used for cell nuclei staining.

Tissue GSL analyses

GSLs in the tissues lysate (cortex, midbrain, liver and lung) were extracted and analyzed by LC/MS at the Lipidomic Core in Medical University of South Carolina. The GSL content was normalized to phosphate content in the same sample after lipid extraction. (GC and GalCer were not separated by LC/MS analysis.) Because 4L;C* mice had normal levels of saposin A and galactosylceramidase, 4L;C* and

WT mice would have the same levels of GalCer. The alterations of GC and GalCer in the analysis will reflect the changes for GC. The data are presented as fold-change of GC in 4L;C* relative to WT after being normalized to phosphate content in the same sample. Hippocampal tissues were analyzed by a modified method in order to separate GC from GalCer at the Lipidomic Core in University of South Carolina. GC, GS and GalCer content in hippocampus were normalized to mg protein in the same samples. Three animals for each genotype were included in the analyses. Data were analyzed by Student's *t*-test.

GCase activity and protein analyses

Mouse tissues were homogenized and their GCase activities were determined fluorometrically with 4MU-Glc in 0.25% Na taurocholate and 0.25% Triton X-100 in the presence and absence of CBE (40). Assay mixtures were incubated for 60 min (37°C). WT control tissues were analyzed in parallel. Mouse liver GCase protein detection by immunoblot was as described (14). The amounts of GCase protein were quantitated by ImageQuant software relative to the amount of β-actin in the same sample. Data were analyzed by Student's *t*-test.

Electrophysiology

LTP was measured using the MED64 multielectrode array (Alpha Med Sciences, Kadoma, Japan) (41) as described previously (39). Animals were anesthetized using isofluorane and decapitated. Brains were removed and placed in an ice cold solution of aCSF. Parasagittal sections (350 μm) of the hippocampus were collected using a vibrotome and transferred to a warm (32°C), constantly oxygenated aCSF bath for a minimum of 1 h. Slices were transferred to the recording chamber, which consists of an 8 × 8 electrode array. Electrodes are 50 μm and are spaced 150 μm apart. Slices were placed so that the CA1 region of the hippocampus was placed across the grid, with recordings coming from the Schaffer collateral pathway. The section was constantly perfused with warmed (32°C) aCSF at a flow rate of 2 mL/min and supplied with humidified 95% O_2/5% CO_2. A stimulation and recording channel were selected out of the 64 possible electrodes. Single-pulse stimuli were delivered from the stimulation channel and the slope of the line from the resulting EPSPs was measured from the defined recording channel. Stimulus amplitude was selected by determining maximum response slope and then selecting a stimulus amplitude that produced a response that was ∼40% of the maximal response. Baseline recordings were collected for a minimum of 10 min. Following baseline, a theta burst stimulus (TBS; 5 Hz for 2 s) was applied to the slice from the stimulation channel. Single-pulse stimuli were again delivered and the resulting EPSPs were collected 1/min for 90 min following TBS. LTP was calculated by taking the percent increase in slope following TBS. Data were analyzed using Performer 2.0 software (Alpha Med Sciences). Six WT and eight 4L;C* mice were used in this study with two slices used per animal. The average of the two slices per animal was used in the subsequent analysis. Data were analyzed using a general linear model ANOVA with gene as a between subject factor and time as a repeated factor.

ACKNOWLEDGEMENTS

The authors thank Venette Inskeep, Matt Zamzow, Brian Quinn and Juying Xu for their technical assistance, Lisa McMillin, Meredith Farmer, Sabina Sylvest, Georgianne Ciraolo and Chris Woods for skilled tissue preparation and photomicrographs, and Brandy Morris for her clerical expertise.

Conflict of Interest statement. None declared.

FUNDING

The authors thank the Lipidomics Core, supported in part by NIH C06 PR018823, at the Medical University of South Carolina. Electrophysiology study was support by a grant to M.T.W. (R01 ES 015689). This work was supported by grants to G.A.G (NS/DK 36681 and DK36729).

REFERENCES

1. Beutler, E. and Grabowski, G.A. (2001). In Scriver, C.R., Beaudet, A.L., Sly, W.S. and Valle, D. (eds), *The Metabolic and Molecular Basis of Inherited Disease*, McGraw-Hill, New York, **Vol. III**, pp. 3635–3668.
2. Grabowski, G.A., Kolodny, E.H., Weinreb, N.J., Rosenbloom, B.E., Prakash-Cheng, A., Kaplan, P., Charrow, J., Pastores, G.M. and Mistry, P.K. (2006). In Scriver, C.R., Sly, W.S., Beaudet, A., Valle, D. and Childs, B. (eds), *The Metabolic and Molecular Bases of Inherited Diseases*, McGraw-Hill, New York.
3. Sidransky, E. (2004) Gaucher disease: complexity in a 'simple' disorder. *Mol. Genet. Metab.*, **83**, 6–15.
4. Orvisky, E., Park, J.K., Parker, A., Walker, J.M., Martin, B.M., Stubblefield, B.K., Uyama, E., Tayebi, N. and Sidransky, E. (2002) The identification of eight novel glucocerebrosidase (GBA) mutations in patients with Gaucher disease. *Hum. Mutat.*, **19**, 458–459.
5. Koprivica, V., Stone, D.L., Park, J.K., Callahan, M., Frisch, A., Cohen, I.J., Tayebi, N. and Sidransky, E. (2000) Analysis and classification of 304 mutant alleles in patients with type 1 and type 3 Gaucher disease. *Am. J. Hum. Genet.*, **66**, 1777–1786.
6. Conradi, N.G., Sourander, P., Nilsson, O., Svennerholm, L. and Erikson, A. (1984) Neuropathology of the Norrbottnian type of Gaucher disease. Morphological and biochemical studies. *Acta. Neuropathol.*, **65**, 99–109.
7. Nilsson, O. and Svennerholm, L. (1982) Accumulation of glucosylceramide and glucosylsphingosine (psychosine) in cerebrum and cerebellum in infantile and juvenile Gaucher disease. *J. Neurochem.*, **39**, 709–718.
8. Orvisky, E., Park, J.K., LaMarca, M.E., Ginns, E.I., Martin, B.M., Tayebi, N. and Sidransky, E. (2002) Glucosylsphingosine accumulation in tissues from patients with Gaucher disease: correlation with phenotype and genotype. *Mol. Genet. Metab.*, **76**, 262–270.
9. Conradi, N.G., Kalimo, H. and Sourander, P. (1988) Reactions of vessel walls and brain parenchyma to the accumulation of Gaucher cells in the Norrbottnian type (type III) of Gaucher disease. *Acta. Neuropathol (Berl).*, **75**, 385–390.
10. Conradi, N.G., Sourander, P., Nilsson, O., Svennerholm, L. and Erikson, A. (1984) Neuropathology of the Norrbottnian type of Gaucher disease. Morphological and biochemical studies. *Acta. Neuropathol (Berl).*, **65**, 99–109.
11. Sandhoff, K., Kolter, T. and Van Echten-Deckert, G. (1998) Sphingolipid metabolism. Sphingoid analogs, sphingolipid activator proteins, and the pathology of the cell. *Ann. N. Y. Acad. Sci.*, **845**, 139–151.
12. Leonova, T., Qi, X., Bencosme, A., Ponce, E., Sun, Y. and Grabowski, G.A. (1996) Proteolytic processing patterns of prosaposin in insect and mammalian cells. *J. Biol. Chem.*, **271**, 17312–17320.

13. Sun, Y., Qi, X. and Grabowski, G.A. (2003) Saposin C is required for normal resistance of acid beta-glucosidase to proteolytic degradation. *J. Biol. Chem.*, **278**, 31918–31923.
14. Sun, Y., Quinn, B., Witte, D.P. and Grabowski, G.A. (2005) Gaucher disease mouse models: point mutations at the acid {beta}-glucosidase locus combined with low-level prosaposin expression lead to disease variants. *J. Lipid Res.*, **46**, 2102–2113.
15. Alattia, J.R., Shaw, J.E., Yip, C.M. and Prive, G.G. (2007) Molecular imaging of membrane interfaces reveals mode of beta-glucosidase activation by saposin C. *Proc. Natl Acad. Sci. USA*, **104**, 17394–17399.
16. Qi, X. and Grabowski, G.A. (2001) Molecular and cell biology of acid beta-glucosidase and prosaposin. *Prog. Nucleic Acid Res. Mol. Biol.*, **66**, 203–239.
17. Tybulewicz, V.L.J., Tremblay, M.L., LaMarca, M.E., Willemsen, R., Stubblefield, B.K., Winfield, S., Zablocka, B., Sidransky, E., Martin, B.M., Huang, S.P. *et al.* (1992) Animal model of Gaucher's disease from targeted disruption of the mouse glucocerebrosidase gene. *Nature*, **357**, 407–410.
18. Willemsen, R., Tybulewicz, V., Sidransky, E., Eliason, W.K., Martin, B.M., LaMarca, M.E., Reuser, A.J., Tremblay, M., Westphal, H., Mulligan, R.C. *et al.* (1995) A biochemical and ultrastructural evaluation of the type 2 Gaucher mouse. *Mol. Chem. Neuropathol.*, **24**, 179–192.
19. Enquist, I.B., Lo Bianco, C., Ooka, A., Nilsson, E., Mansson, J.E., Ehinger, M., Richter, J., Brady, R.O., Kirik, D. and Karlsson, S. (2007) Murine models of acute neuronopathic Gaucher disease. *Proc. Natl Acad. Sci. USA*, **104**, 17483–17488.
20. Xu, Y.H., Reboulet, R., Quinn, B., Huelsken, J., Witte, D. and Grabowski, G.A. (2008) Dependence of reversibility and progression of mouse neuronopathic Gaucher disease on acid beta-glucosidase residual activity levels. *Mol. Genet. Metab.*, **94**, 190–203.
21. Sun, Y., Qi, X., Witte, D.P., Ponce, E., Kondoh, K., Quinn, B. and Grabowski, G.A. (2002) Prosaposin: threshold rescue and analysis of the 'neuritogenic' region in transgenic mice. *Mol. Genet. Metab.*, **76**, 271–286.
22. Xu, Y.H., Quinn, B., Witte, D. and Grabowski, G.A. (2003) Viable mouse models of acid beta-glucosidase deficiency: the defect in Gaucher disease. *Am. J. Pathol.*, **163**, 2093–2101.
23. Sun, Y., Ran, H., Zamzow, M., Kitatani, K., Skelton, M.R., Williams, M.T., Vorhees, C.V., Witte, D.P., Hannun, Y.A. and Grabowski, G.A. (2009) Specific saposin C deficiency: CNS impairment and acid {beta}-glucosidase effects in the mouse. *Hum. Mol. Genet.*, December 17, Epub ahead of print.
24. Eskelinen, E.L. (2006) Roles of LAMP-1 and LAMP-2 in lysosome biogenesis and autophagy. *Mol. Aspects Med.*, **27**, 495–502.
25. Kirkin, V., Lamark, T., Johansen, T. and Dikic, I. (2009) NBR1 cooperates with p62 in selective autophagy of ubiquitinated targets. *Autophagy*, **5**, 732–733.
26. Kaye, E.M., Ullman, M.D., Wilson, E.R. and Barranger, J.A. (1986) Type 2 and type 3 Gaucher disease: a morphological and biochemical study. *Ann. Neurol.*, **20**, 223–230.
27. Cervos-Navarro, J. and Zimmer, C. (1990) Light microscopic and ultrastructural study on CNS lesions in infantile Gaucher's disease. *Clin. Neuropathol.*, **9**, 310–313.
28. Conradi, N., Kyllerman, M., Mansson, J.E., Percy, A.K. and Svennerholm, L. (1991) Late-infantile Gaucher disease in a child with myoclonus and bulbar signs: neuropathological and neurochemical findings. *Acta Neuropathol.*, **82**, 152–157.
29. Orvisky, E., Sidransky, E., McKinney, C.E., Lamarca, M.E., Samimi, R., Krasnewich, D., Martin, B.M. and Ginns, E.I. (2000) Glucosylsphingosine accumulation in mice and patients with type 2 Gaucher disease begins early in gestation. *Pediatr. Res.*, **48**, 233–237.
30. Wong, K., Sidransky, E., Verma, A., Mixon, T., Sandberg, G.D., Wakefield, L.K., Morrison, A., Lwin, A., Colegial, C., Allman, J.M. *et al.* (2004) Neuropathology provides clues to the pathophysiology of Gaucher disease. *Mol. Genet. Metab.*, **82**, 192–207.
31. Schueler, U.H., Kolter, T., Kaneski, C.R., Blusztajn, J.K., Herkenham, M., Sandhoff, K. and Brady, R.O. (2003) Toxicity of glucosylsphingosine (glucopsychosine) to cultured neuronal cells: a model system for assessing neuronal damage in Gaucher disease type 2 and 3. *Neurobiol. Dis.*, **14**, 595–601.
32. Pelled, D., Trajkovic-Bodennec, S., Lloyd-Evans, E., Sidransky, E., Schiffmann, R. and Futerman, A.H. (2005) Enhanced calcium release in the acute neuronopathic form of Gaucher disease. *Neurobiol. Dis.*, **18**, 83–88.
33. Lloyd-Evans, E., Pelled, D., Riebeling, C., Bodennec, J., de-Morgan, A., Waller, H., Schiffmann, R. and Futerman, A.H. (2003) Glucosylceramide and glucosylsphingosine modulate calcium mobilization from brain microsomes via different mechanisms. *J. Biol. Chem.*, **278**, 23594–23599.
34. Kacher, Y. and Futerman, A.H. (2006) Genetic diseases of sphingolipid metabolism: pathological mechanisms and therapeutic options. *FEBS Lett.*, **580**, 5510–5517.
35. Vaccaro, A.M., Muscillo, M. and Suzuki, K. (1985) Characterization of human glucosylsphingosine glucosyl hydrolase and comparison with glucosylceramidase. *Eur. J. Biochem.*, **146**, 315–321.
36. Matsuda, J., Vanier, M.T., Saito, Y., Tohyama, J. and Suzuki, K. (2001) A mutation in the saposin A domain of the sphingolipid activator protein (prosaposin) gene results in a late-onset, chronic form of globoid cell leukodystrophy in the mouse. *Hum. Mol. Genet.*, **10**, 1191–1199.
37. Sun, Y., Witte, D.P., Zamzow, M., Ran, H., Quinn, B., Matsuda, J. and Grabowski, G.A. (2007) Combined saposin C and D deficiencies in mice lead to a neuronopathic phenotype, glucosylceramide and alpha-hydroxy ceramide accumulation, and altered prosaposin trafficking. *Hum. Mol. Genet.*, **16**, 957–971.
38. Ferguson, C.J., Lenk, G.M. and Meisler, M.H. (2009) Defective autophagy in neurons and astrocytes from mice deficient in PI(3,5)P2. *Hum. Mol. Genet.*, **18**, 4868–4878.
39. Sun, Y., Witte, D.P., Ran, H., Zamzow, M., Barnes, S., Cheng, H., Han, X., Williams, M.T., Skelton, M.R., Vorhees, C.V. *et al.* (2008) Neurological deficits and glycosphingolipid accumulation in saposin B deficient mice. *Hum. Mol. Genet.*, **17**, 2345–2356.
40. Xu, Y.H., Ponce, E., Sun, Y., Leonova, T., Bove, K., Witte, D. and Grabowski, G.A. (1996) Turnover and distribution of intravenously administered mannose-terminated human acid beta-glucosidase in murine and human tissues. *Pediatr. Res.*, **39**, 313–322.
41. Shimono, K., Baudry, M., Ho, L., Taketani, M. and Lynch, G. (2002) Long-term recording of LTP in cultured hippocampal slices. *Neural. Plast.*, **9**, 249–254.